A Decoupling Technique for Four-Element Symmetric Arrays With Reactively Loaded Dummy Elements

Luyu Zhao and Ke-Li Wu

***Abstract*—A decoupling technique for a symmetric four-element compact array is proposed. A dummy array terminated with optimum reactive loads is introduced to cancel the mutual couplings between the four radiating elements. A theory that leads to a general design procedure is developed. The technique is demonstrated by three practical design examples, including a compact and low-profile "cheese-cake" antenna array. Calculated channel capacities demonstrate that the performance of a 4-by-4 MIMO communication system that uses the cheese-cake array can be significantly improved as compared to the system using its coupled counterpart. This technique provides a promising approach to the design of a compact four-element array for a MIMO communication system.**

***Index Terms*—Antenna decoupling, compact antenna array, LTE-advanced, multiple-input-multiple-output (MIMO), mutual coupling.**

I. Introduction

With the fast evolution of next generation communication systems, the demand for high data rate is dramatically increasing. The LTE-Advanced requires data rate of more than 1 Gbps [1]. Despite that M-by-2 MIMO systems have been in commercial use, the potential use of higher order MIMO systems are under development. Theoretically, an M-by-4 MIMO system provides more leverage than a conventional M-by-2 system in terms of complexity of the system, date rate and reliability, where M is the number of antennas on base stations.

However, as the number of antenna elements increases in a compact wireless device, the electric distance between antenna elements decreases, and mutual coupling as well as pattern correlation increase [2]. In an M-by-4 MIMO system, strong mutual couplings between antenna elements inevitably reduce signal-to-noise ratio and antenna efficiency. Furthermore, the channel capacity can be greatly affected in a highly correlated channel. These drawbacks limit the benefits of a MIMO system. Therefore, it is vital that a simple but effective decoupling technique is developed for a multiple antenna system.

Very few existing decoupling techniques can effectively deal with a decoupling problem of a compact array with more than two elements. The most obvious method is to apply conventional two-element decoupling techniques to every pair of elements in the array. Such techniques include the electromagnetic band gap (EBG) structures [3], the defected ground structures [4], [5], the inserted transmission lines [6], and the coupled resonator decoupling networks [7]. But these methods will lead to complex circuitry when applied to a multi-element array. Another method is to use a mode-decomposition network that diagonalizes the S-parameters of a coupled array. This decoupling technique is relatively narrow band and the efficiencies and Qs for the respective modes are quite different [8]–[11]. The polarization diversity technique for a four-element MIMO array is also a choice [12]. For multiple element arrays, utilizing the polarization diversity to achieve decoupling is not easy because only limited polarization degrees of freedom are available. Recently, a decoupling technique using a parasitic scatterer was reported in [13]; this technique is only proved to be applicable for two-element arrays or equilateral triangular arrays.

This communication will present a decoupling technique for a compact array of four elements. The theory and design procedures are developed in Section II and three design examples are presented in Section III. Section IV concludes the communication.

Manuscript received May 14, 2013; revised March 19, 2014; accepted May 10, 2014. Date of publication June 02, 2014; date of current version July 31, 2014. This work was supported in part by a Postgraduate scholarship of The Chinese University of Hong Kong and by the Development and Reform Commission of Shenzhen Municipality under Grant Shen Fa Gai (2013) 1673. *(Corresponding author: K.-L. Wu).*

The authors are with the Department of Electronic Engineering, The Chinese University of Hong Kong, Shatin, NT, Hong Kong and also with the Shenzhen Engineering Laboratory of Wireless Locating Technology and System, Shenzhen Research Institute, The Chinese University of Hong Kong (e-mail: lyzhao@ee.cuhk.edu.hk; klwu@ee.cuhk.edu.hk).

Color versions of one or more of the figures in this communication are available online at http://ieeexplore.ieee.org.

Digital Object Identifier 10.1109/TAP.2014.2326425

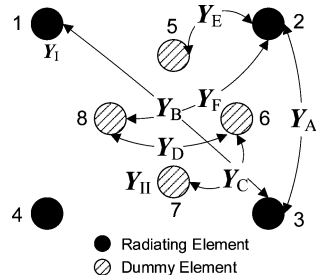

Fig. 1. The configuration diagram of a four-element array with four dummy elements.

II. Theory

A. Network Representation

To decouple a symmetric compact four-element array, a uniform four-element dummy array is placed at the center of the compact array with its layout rotated by 45° as shown in Fig. 1. Antenna elements 1–4 are radiating elements and elements 5–8 are dummy elements that are terminated with reactive loads. There are six distinct *short-circuit* mutual admittances:

Y_A : Admittance between adjacent radiating elements;
Y_B : Admittance between diagonal radiating elements;
Y_C : Admittance between adjacent dummy elements;
Y_D : Admittance between diagonal dummy elements;
Y_E : Admittance between a radiating element and a nearby dummy element; and
Y_F : Admittance between a radiating element and a distant dummy element.

There are also two self-admittances:

$\mathrm{Y_I}$: The self-admittance of a radiating element; and
$\mathrm{Y_{II}}$: The self-admittance of a dummy element.

Consider the voltage-current relation of the eight antenna elements as shown in Fig. 2(a):

$$\begin{bmatrix} \overline{\mathbf{I}}_1 \\ \overline{\mathbf{I}}_2 \end{bmatrix} = \begin{bmatrix} \overline{\mathbf{Y}}_{11} & \overline{\mathbf{Y}}_{12} \\ \overline{\mathbf{Y}}_{21} & \overline{\mathbf{Y}}_{22} \end{bmatrix} \cdot \begin{bmatrix} \overline{\mathbf{V}}_1 \\ \overline{\mathbf{V}}_2 \end{bmatrix} \tag{1}$$

where

$$\overline{\mathbf{I}}_1 = \begin{bmatrix} i_1 \\ i_2 \\ i_3 \\ i_4 \end{bmatrix}, \quad \overline{\mathbf{I}}_2 = \begin{bmatrix} i_5 \\ i_6 \\ i_7 \\ i_8 \end{bmatrix}$$

$$\overline{\mathbf{V}}_1 = \begin{bmatrix} v_1 \\ v_2 \\ v_3 \\ v_4 \end{bmatrix}, \quad \overline{\mathbf{V}}_2 = \begin{bmatrix} v_5 \\ v_6 \\ v_7 \\ v_8 \end{bmatrix} \tag{2a}$$

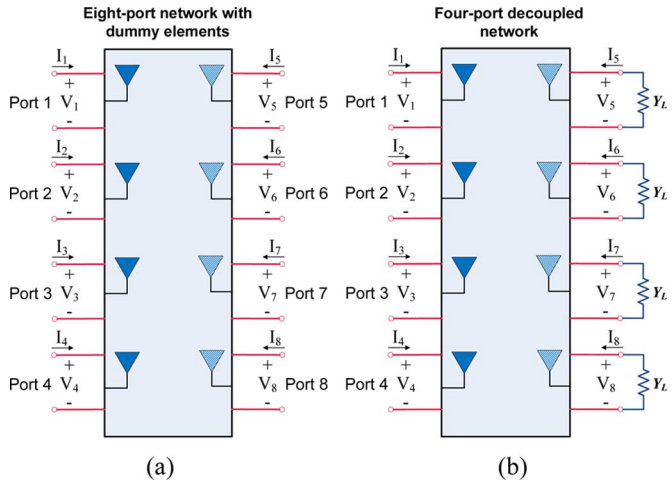

Fig. 2. (a) The eight-port network consists of four radiating elements and four dummy elements. (b) The four port network where the dummy elements are terminated with load Y_L.

and

$$\overline{\mathbf{Y}}_{11} = \begin{bmatrix} Y_{\mathrm{I}} & Y_A & Y_B & Y_A \\ Y_A & Y_{\mathrm{I}} & Y_A & Y_B \\ Y_B & Y_A & Y_{\mathrm{I}} & Y_A \\ Y_A & Y_B & Y_A & Y_{\mathrm{I}} \end{bmatrix}$$

$$\overline{\mathbf{Y}}_{12} = \begin{bmatrix} Y_E & Y_F & Y_F & Y_E \\ Y_E & Y_E & Y_F & Y_F \\ Y_F & Y_E & Y_E & Y_F \\ Y_F & Y_F & Y_E & Y_E \end{bmatrix} \tag{2b}$$

$$\overline{\mathbf{Y}}_{21} = \begin{bmatrix} Y_E & Y_E & Y_F & Y_F \\ Y_F & Y_E & Y_E & Y_F \\ Y_F & Y_F & Y_E & Y_E \\ Y_E & Y_F & Y_F & Y_E \end{bmatrix}$$

$$\overline{\mathbf{Y}}_{22} = \begin{bmatrix} Y_{\mathrm{II}} & Y_C & Y_D & Y_C \\ Y_C & Y_{\mathrm{II}} & Y_C & Y_D \\ Y_D & Y_C & Y_{\mathrm{II}} & Y_C \\ Y_C & Y_D & Y_C & Y_{\mathrm{II}} \end{bmatrix}. \tag{2c}$$

If each dummy element is terminated by a load Y_L as shown in Fig. 2(b), the voltage-current relation at the ports of the dummy elements can be described by

$$\overline{\mathbf{I}}_2 = \overline{\mathbf{Y}}_L \cdot \overline{\mathbf{V}}_2 \tag{3}$$

with

$$\overline{\mathbf{Y}}_L = \mathrm{diag}[-Y_L, -Y_L, -Y_L, -Y_L]. \tag{4}$$

Substituting (3) into (1) yields

$$\overline{\mathbf{I}}_1 = [\overline{\mathbf{Y}}_{11} - \overline{\mathbf{Y}}_{12}(\overline{\mathbf{Y}}_{22} - \overline{\mathbf{Y}}_L)^{-1}\overline{\mathbf{Y}}_{21}] \cdot \overline{\mathbf{V}}_1. \tag{5}$$

Taking all dummy elements and their respective loads into account, the voltage-current relation between the four radiating elements can be expressed as

$$\begin{bmatrix} i_1 \\ i_2 \\ i_3 \\ i_4 \end{bmatrix} = \begin{bmatrix} Y_{\mathrm{I}}^{'} & Y_A^{'} & Y_B^{'} & Y_A^{'} \\ Y_A^{'} & Y_{\mathrm{I}}^{'} & Y_A^{'} & Y_B^{'} \\ Y_B^{'} & Y_A^{'} & Y_{\mathrm{I}}^{'} & Y_A^{'} \\ Y_A^{'} & Y_B^{'} & Y_A^{'} & Y_{\mathrm{I}}^{'} \end{bmatrix} \cdot \begin{bmatrix} v_1 \\ v_2 \\ v_3 \\ v_4 \end{bmatrix}. \tag{6}$$

Substituting (2) and (4) into (5) and comparing with (6), it is apparent that by terminating the dummy elements by load Y_L, the original short-circuit admittances of the radiating elements are modified to

$$Y_{\mathrm{I}}^{'} = Y_{\mathrm{I}} - \frac{(Y_E + Y_F)^2}{Y_{\mathrm{II}} + Y_L + 2Y_C + Y_D} - \frac{(Y_E - Y_F)^2}{Y_{\mathrm{II}} + Y_L - Y_D} \tag{7a}$$

$$Y_A^{'} = Y_A - \frac{(Y_E + Y_F)^2}{Y_{\mathrm{II}} + Y_L + 2Y_C + Y_D}, \tag{7b}$$

and

$$Y_B^{'} = Y_B - \frac{(Y_E + Y_F)^2}{Y_{\mathrm{II}} + Y_L + 2Y_C + Y_D} + \frac{(Y_E - Y_F)^2}{Y_{\mathrm{II}} + Y_L - Y_D}. \tag{7c}$$

Equation (7) states that by appropriately controlling the mutual couplings between dummy elements, the dummy and radiating elements as well as the load Y_L, all the mutual couplings between the radiating elements in the original array can be cancelled out in certain extent.

B. Design Procedures of Dummy Array

It is clear that to decouple the four symmetric radiating elements, (7b) and (7c) should equal to zero at the same time, which will lead to two simultaneous equations. Solving $Y_A^{'} = 0$ directly will lead to one load condition

$$Y_{L1} = \frac{(Y_E + Y_F)^2}{Y_A} - Y_{\mathrm{II}} - 2Y_C - Y_D. \tag{8}$$

Meanwhile, solving $(7c) = 0$ can also yield another load condition. However, since there is one common term in both (7b) and (7c), it is more convenient to subtract (7b) by (7c) in order to find another condition

$$Y_{L2} = \frac{(Y_E - Y_F)^2}{Y_A - Y_B} - Y_{\mathrm{II}} + Y_D. \tag{9}$$

It can be seen from (8) and (9) that in general $Y_{L1} \neq Y_{L2}$, which means that the values of Y_C, Y_D, Y_E, Y_F and Y_{II} in (8) and (9) must be properly designed to ensure that Y_{L1} are close to Y_{L2} in the first place. In a practical design, these values depend on the relative spacing between the radiating elements and the dummy elements as well as the form factors of the dummy array. Theoretically, there are two major steps to find a load that can optimally satisfy (8) and (9) simultaneously within the frequency band of interest: step 1 is to optimize the form factors of the dummy array, such as the element spacing, such that Y_{L1} and Y_{L2} are most close to each other; and step 2 is to find an optimal load such that (8) and (9) are best satisfied in the frequency band of interest. Therefore, the effectiveness of the decoupling is dominated by the difference of the two conditions within the frequency band of interest. In general, the optimum load is a complex number. However, for a complex load whose real part is relatively small, using a purely reactive load is an effective approximation.

Having found the dummy element configuration from a wide range of selections, one can find an optimum reactive load value Y_{Lopt} that achieves a minimum difference by a simple optimization search. If a reactive load Y_L is realized by a section of open ended transmission line, the load is given by $Y_L = jY_0 \tan \beta l$, where Y_0 and β are the characteristic admittance and phase constant of the transmission line, and l is the length of the line obtained by optimization. The goal function for searching the optimal length that best satisfies $Y_A^{'}, Y_B^{'} = 0$ simultaneously can be defined by minimizing the following function:

$$g(l) = \frac{w_1 \cdot \sum_{i=1}^{N_s} |Y_A'(f_i)|^2 + w_2 \cdot \sum_{i=1}^{N_s} |Y_B'(f_i)|^2}{g(l)_{\max}} \tag{10}$$

where w_1 and w_2 are normally chosen to be 1, N_s is the number of sampling frequency points f_i selected in the frequency band of interest. The goal function is normalized to the maximum value of $g(l)$, $g(l)_{\max}$

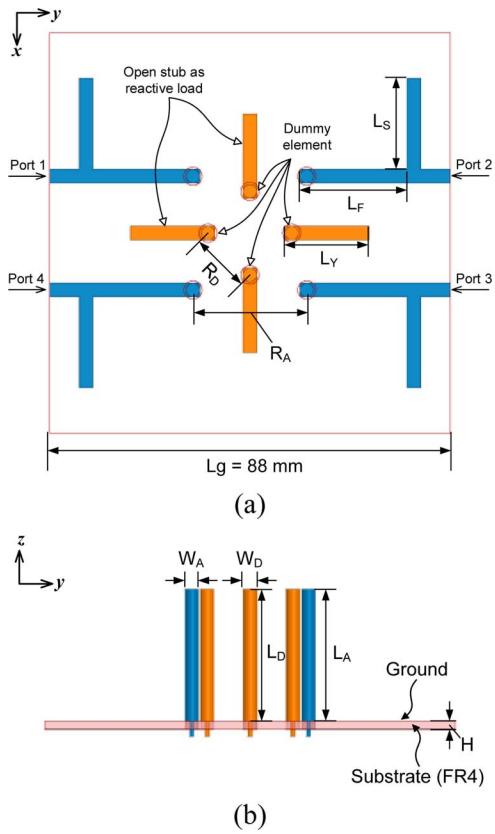

Fig. 3. (a) Top view and (b) front view of a four-element coupled monopole array together with a four-element dummy array terminated by open ended transmission lines.

because admittance parameter tends to be singular at poles and a large value of the goal function will desensitize the optimization process.

III. Design Examples and Design Considerations

Three design examples are presented in this section. In the first two examples, the same four-element coupled array is decoupled using two different decoupling dummy arrays, which differ in the spacing and load values. Then a novel "cheese-cake" four-element PIFA array is proposed.

A. Four-Element Cylindrical Monopole Arrays

A four-element monopole circular array with inter-element spacing $R_A = 25$ mm ($0.21\lambda_0$ at 2.6 GHz) shown in Fig. 3 is considered in this example. Due to the limited electric distances between elements, the isolations between the adjacent and the diagonal elements as well as the return losses of each element are poor. If the array is matched at 2.6 GHz with extra matching stubs, the isolations become even worse. As is shown in Fig. 4(a), the isolations between the adjacent elements and diagonal elements for the coupled array at the center frequency are around 10 dB and 15 dB, respectively. For clarity, the detailed design process will be given step by step:

Step 1: Designing a Dummy Array: In this example, the four dummy monopoles are chosen to be identical to the radiating elements, although different dummy antenna form factors are also possible. The combined array incorporating four *unmatched* radiating elements and four dummy elements can be treated as an eight-port network as shown in Fig. 2(a), whose S-parameters are obtained by a full-wave EM simulation [14]. In the simulation, the conductivity is set to 1.5×10^7 siements/m and the loss tangent of the substrate is set to 0.02. Obviously, the S-parameters of the radiating array depend on not only the geometries of radiating and dummy elements, but also on the relative locations of the dummy elements with respect to the radiating elements, the reactive load and the ground size.

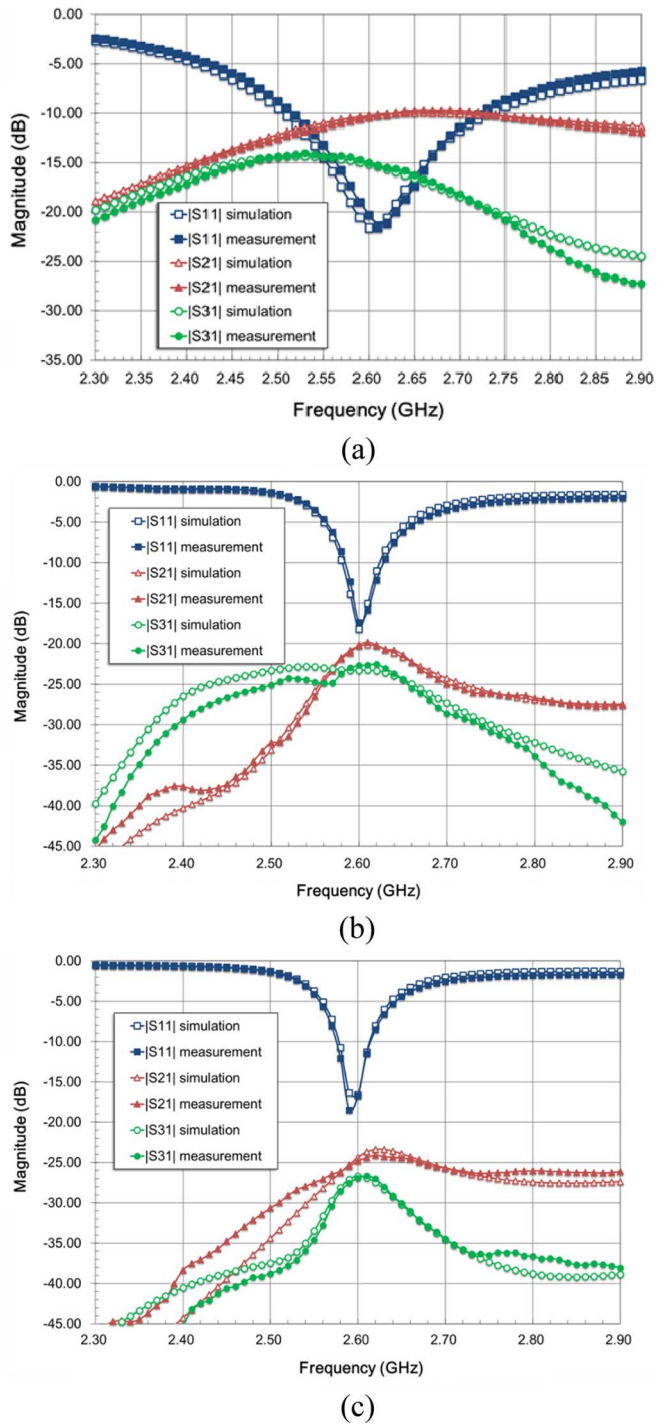

Fig. 4. The simulated and measured S-parameters of the four-element monopole array: (a) matched but coupled array; (b) decoupled Array 1; and (c) decoupled Array 2.

For convenience, load impedances $Z_L = 1/Y_L$, $Z_{L1} = 1/Y_{L1}$ and $Z_{L2} = 1/Y_{L2}$ are used in the following discussions. Denote the difference of the two loads as $Z_{\mathrm{Ld}} = Z_{L1} - Z_{L2}$ and the space between two adjacent dummy elements as R_D. To illustrate the relation

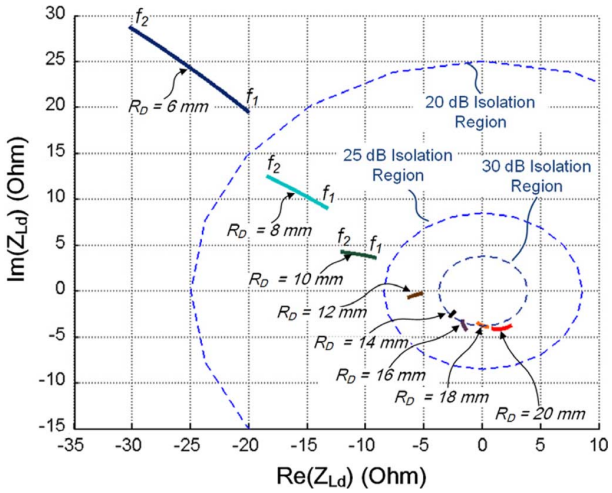

Fig. 5. Z_{Ld} in a given frequency range ($\mathrm{f}_1 = 2.55$ GHz, $\mathrm{f}_2 = 2.65$ GHz) for different dummy element configuration parameter R_D and different illustrative isolation contours.

between Z_{Ld} and the worst isolations between the radiating elements, several arrays with different R_D are simulated and the locus of Z_{Ld} in a given frequency band for different spacing value R_D is calculated according to (8) and (9) and they are then plotted in Fig. 5. Illustrative contours for different isolation levels are also superposed in the figure. It should be noted that the illustrative isolation contours account for both the adjacent and diagonal isolations. Therefore, if Z_{Ld} is large, the worst isolation becomes dominant. Consequently, the dummy array becomes less effective. It is also observed that the larger the spacing of the dummy elements, the smaller the difference in Z_{Ld}. In fact, the observation is consistent with the physical interpretation that when the distance between two dummy elements is large, the difference between Y_E and Y_F also becomes large, so that the difference between Y_A and Y_B can be effectively compensated. It has been demonstrated, through this example, that to decouple an array with multiple elements using reactive loaded dummy elements, there is no exact solution in general. Designing a decoupling network becomes a trade-off between the achievable isolation and the dimension of the whole array.

Step 2: Optimizing the Reactive Load: Once the dummy array configuration is chosen, the reactive load can be obtained by minimizing the worst isolation between the radiating elements. It is apparent that for a given coupled array, different optimum loads are available for different dummy array configurations. For one solution (named Array 1), the side-by-side spacing R_D of the dummy array is chosen to be 12 mm. For another solution (named Array 2), $R_D = 18$ mm is used. The load value against the normalized goal function defined by (10) is plotted in Fig. 6, where the maximum value of the goal function for both Array 1 and Array 2 is used to normalize the goal function. It is observed that the optimum reactive load Z_L for Array 1 and Array 2 are $-j12.5$ Ohms and $-j8.5$ Ohms, respectively. The dimensions of the two arrays are summarized in Table I.

Step 3: Designing Matching Networks: As stated by (7a), decoupling of a radiating array will affect its matching performance. Therefore, a matching network is needed at each port after the array is decoupled. Since the radiating elements are isolated to each other after decoupling, each port can be matched independently. For the decoupled monopole arrays, matching stubs are used.

The simulation and measurement results for decoupled Array 1 and Array 2 are shown in Fig. 4(b) and (c). It can be seen that the adjacent and diagonal isolations at the center frequency are around 20 dB and 23 dB for Array 1, and 25 dB and 27 dB for Array 2, respectively. The

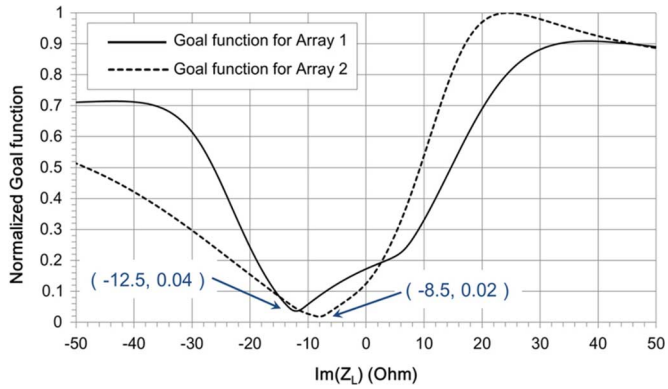

Fig. 6. The normalized goal functions versus load Z_L for Array 1 and Array 2.

TABLE I
DIMENSIONS OF THE FOUR-ELEMENT MONOPOLE ARRAY (UNIT: MM)

	Decoupled array 1	Decoupled array 2
R_A	25.0	25.0
R_D	12.0	18.0
L_Y	13.0	14.7
L_F	26.5	26.5
L_S	19.0	20.0
L_A, L_D	27.0	27.0
W_A, W_D	3	3

fractional bandwidths for isolations below 20 dB are more than 50%. The fractional bandwidths for a return loss better than 6 dB are better than 3%. It is understandable that when the isolation is improved, antenna efficiency and Q factor increase and, consequently, the matching bandwidth decreases. It can be shown, in the following example, that decoupling of a broad band four-element array is also possible using different form factors of the elements and array configurations.

B. A Four-Element "Cheese-Cake" PIFA Array

When deploying an indoor MIMO system by a distributed antenna system (DAS), the required antenna arrays need to be compact, low-profile, high efficiency, and yet with acceptable bandwidth. To meet the requirements, a "cheese-cake" antenna array is proposed. As shown in Fig. 7, the antenna array consists of four planar inverted F radiating antennas (PIFAs) and four planar inverted F dummy elements. As there are sufficient geometric parameters in the dummy array to be tuned, to maintain a relative simple structure, four simple grounded dummy elements are preferred in this case. In other words, the load impedance should be zero. To decouple the adjacent and diagonal mutual couplings in this example, parameters $F2$, $P2$ and L_{FD} are fixed and R_D is tunable. A number of radiating and dummy array compositions with different R_D are examined. For each composition, the relation of the load and the normalized goal functions defined in (10) is plotted in Fig. 8. It can be observed from Fig. 8 that the dummy array with $R_D = 30$ mm will have an optimum load impedance of zero, which means that short-circuited dummy elements are sufficient to cancel out all the unwanted mutual couplings.

Having had an appropriate configuration of the short- circuited dummy array, the radiating elements are isolated from each other. Extra matching networks can further improve the matching performance.

The final layout of the cheese-cake antenna array is depicted in Fig. 7 with the dimensions listed in Table II. To better evaluate the performance of the cheese-cake array, a coupled array as shown in Fig. 7(b) is designed with the best effort under the constraint of similar dimensions and structure. The measured and the simulated S-parameters of the

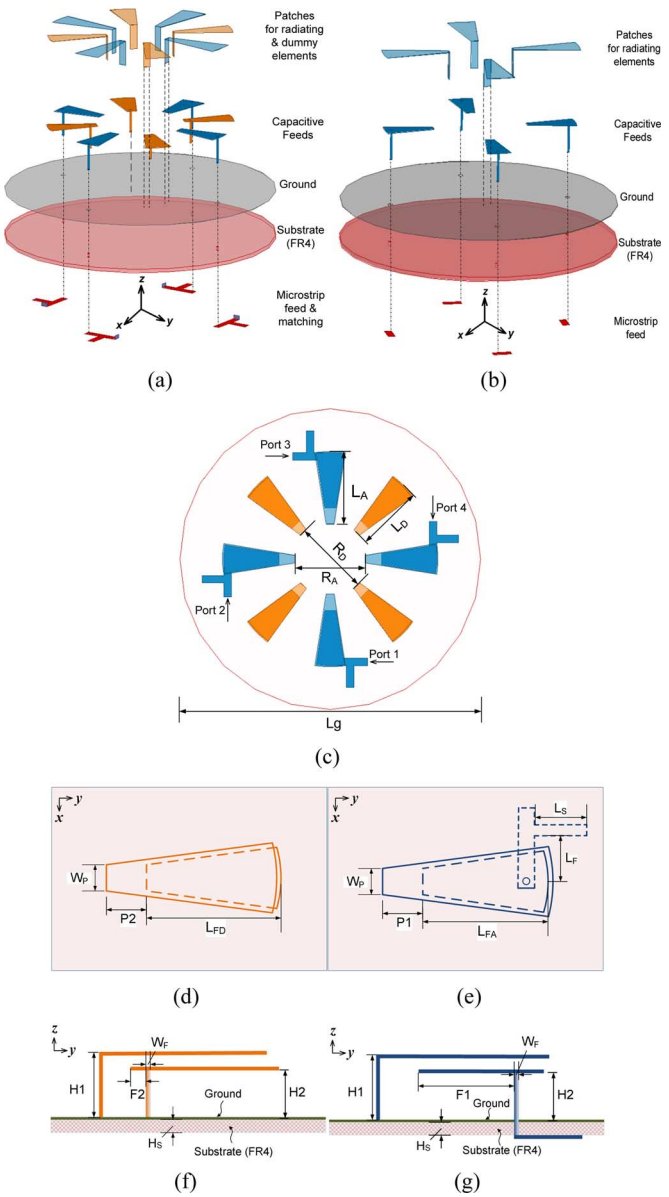

Fig. 7. The view of (a) the cheese-cake array; (b) the coupled array; (c) top view of the cheese-cake antenna array; (d) top view of a dummy element; (e) the top view of a radiating element; (f) side view of a dummy element and (g) the side view of a radiating element.

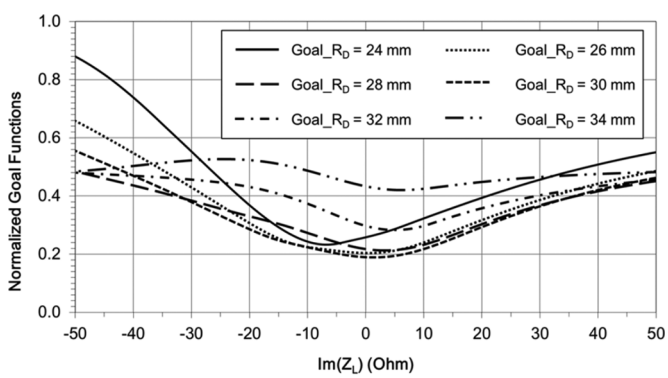

Fig. 8. The goal functions normalized to the largest goal value of all the cases versus the load Z_L with different R_D values.

cheese-cake array and the coupled array are superposed in Fig. 9. The decoupling performance with $|S_{21}| \leq -20$ dB and $|S_{31}| \leq -26$ dB

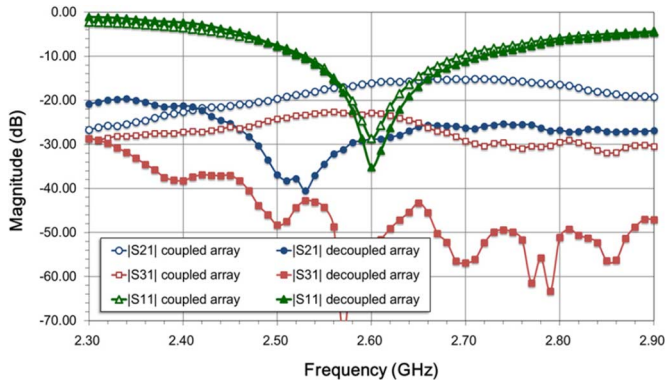

Fig. 9. Measured magnitude of scattering parameters of the coupled and the decoupled cheese-cake array.

TABLE II
DIMENSIONS OF THE CHEESECAKE ANTENNA ARRAY (UNIT: MM)

Variables	Size	Variables	Size
L_g	120	H1	11
R_D	30	H2	10.2
R_A	28	P1	6.5
L_A	29	F1	20
L_D	26	P2	4.5
L_{FA}, L_{FD}	22	F2	3

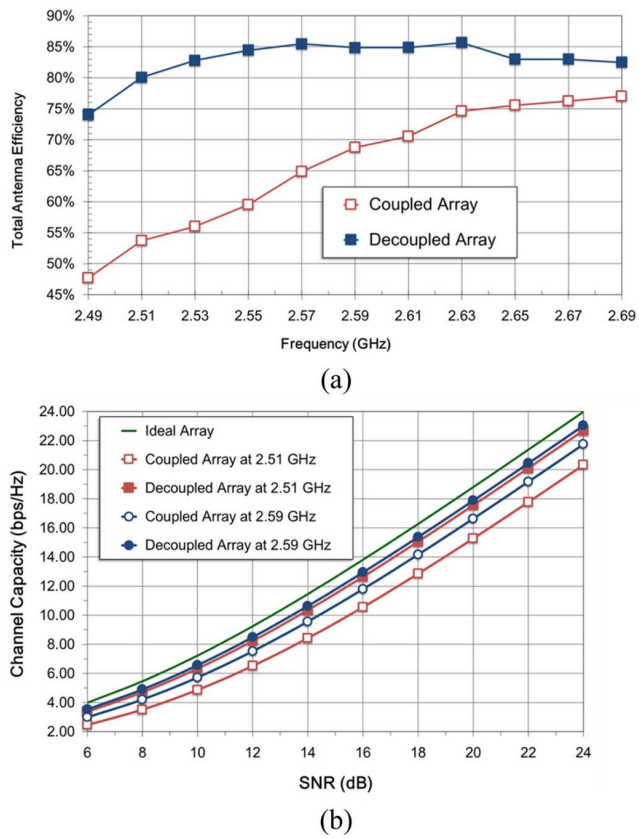

Fig. 10. (a) Measured total antenna efficiencies (including reflection losses and averaging of four radiating elements); (b) channel capacity and comparison between the cheese-cake array and its coupled counterpart.

is achieved from 2.3 GHz to 2.9 GHz. The matching bandwidth with $|S_{11}| \leq -10$ dB is 196 MHz, which is sufficiently large for the required downlink and uplink bands of the LTE 2.6 GHz-band.

The radiation characteristics of the cheese-cake antenna array together with its coupled counterpart are measured using the SATIMO

SG128 spherical near-field scanner in the ISO17025 accredited Radiofrequency Radiation Research Laboratory of The Chinese University of Hong Kong. The radiation pattern of each element is directive with peak gain of 5.88 dBi and is not shown due to limited page space. Nevertheless, the total efficiencies for the cheese-cake array and its coupled counterpart are superposed in Fig. 10(a). Within the band of interest, the total efficiencies are improved from 67% to 85%.

The channel capacities for the decoupled cheesecake array, its coupled counterpart and an ideal 4-by-4 MIMO array with respect to different SNRs are calculated and are superposed in Fig. 10(b). The calculation follows the method proposed in [15], which takes the antenna efficiency and the correlation coefficient into considerations. The receiver is assumed to be uncorrelated, and the cheese-cake array and its coupled counterpart are placed at the transmitter. The average improvement in the channel capacity of the cheese-cake array as compared to its coupled counterpart is 2.01 bps/Hz at 2.51 GHz and 1.15 bps/Hz at 2.59 GHz.

IV. Conclusion

The communication presents a decoupling technique for a four-element symmetric antenna array. A theory that leads to a general design procedure is developed from the network point of view. Based on the decoupling technique, a low-profile wideband cheese-cake antenna array is proposed. The array possesses good isolation and matching performances simultaneously as well as low correlations. Channel capacity is also obtained through the measured data. The proposed decoupling technique provides an effective way to decouple a compact four-element symmetric array of any form factor, enhances the radiation efficiency and ultimately improves channel capacity for a MIMO communication system. Although only symmetric arrays are discussed, the theory has the potential to be extended to asymmetric arrays.

References

[1] 3GPP TR 36.913, V11.0.0, "Requirements for further advancements for evolved universal terrestrial radio access (E-UTRA) (LTE-Advanced)," Nov. 2012.

[2] M. A. Jensen and J. W. Wallace, "A review of antennas and propagation for MIMO wireless communications," *IEEE Trans. Antennas Propag.*, vol. 52, no. 11, pp. 2810–2824, Nov. 2004.

[3] F. Yang and Y. R. Samii, "Microstrip antennas integrated with electromagnetic band-gap EBG structures: A low mutual coupling design for array applications," *IEEE Trans. Antennas Propag.*, vol. 51, no. 10, pp. 2936–2946, Oct. 2003.

[4] C. Y. Chiu, C. H. Cheng, R. D. Murch, and C. R. Rowell, "Reduction of mutual coupling between closely-packed antenna element," *IEEE Trans. Antennas Propag.*, vol. 55, no. 6, pp. 1732–1738, Jun. 2007.

[5] H. Li, J. Xiong, and S. He, "A compact planar MIMO antenna system of four elements with similar radiation characteristics and isolation structure," *IEEE Antennas Wireless Propag. Lett.*, vol. 8, pp. 1107–1110, 2009.

[6] J. B. Andersen and H. H. Rasmussen, "Decoupling and descattering networks for antennas," *IEEE Trans. Antennas Propag.*, vol. 24, no. AP-6, pp. 841–846, Nov. 1976.

[7] L. Zhao, L. K. Yeung, and K.-L. Wu, "A coupled resonator decoupling network for two-element compact antenna arrays in mobile terminals," *IEEE Trans. Antennas Propag.*, vol. 62, no. 5, pp. 2767–2776, May 2014.

[8] C. Volmer, J. Weber, R. Stephan, K. Blau, and M. A. Hein, "An eigenanalysis of compact antenna arrays and its application to port decoupling," *IEEE Trans. Antennas Propag.*, vol. 56, no. 2, Feb. 2008.

[9] L. K. Yeung and Y. E. Wang, "Mode-based beamforming arrays for miniaturized platforms," *IEEE Trans. Microw. Theory Tech.*, vol. 57, no. 1, pp. 45–52, Jan. 2009.

[10] J. C. Coetzee and Y. Yu, "Port decoupling for small arrays by means of an eigenmode feed network," *IEEE Trans. Antennas Propag.*, vol. 56, no. 6, pp. 1587–1593, Jun. 2008.

[11] J. C. Coetzee and Y. Yu, "New modal feed network for a compact monopole array with isolated ports," *IEEE Trans. Antennas Propag.*, vol. 56, no. 12, pp. 3872–3875, Dec. 2008.

[12] A. S. Konanur, K. Gosalia, S. H. Krishnamurthy, B. Hughes, and G. Lazzi, "Increasing wireless channel capacity through MIMO systems employing co-located antennas," *IEEE Trans. Microw. Theory Tech.*, vol. 53, pp. 1837–1844, Jun. 2005.

[13] B. K. Lau and J. B. Andersen, "Simple and efficient decoupling of compact arrays with parasitic scatterers," *IEEE Trans. Antennas Propag.*, vol. 60, no. 2, pp. 464–472, Feb. 2012.

[14] EMPro 3D EM Simulation Software, Version 2012.09, Agilent Technologies, Inc. Santa Clara, CA, USA.

[15] J. X. Yun and R. G. Vaughan, "Multiple element antenna efficiency and impact on diversity and capacity," *IEEE Trans. Antennas Propag.*, vol. 60, no. 2, pp. 529–539, Feb. 2012, pt. I.

A Hybrid E-pulse Method for Discrimination of Conducting Scatterers in Resonance Region

Dhiraj K. Singh, Naveena Mohan, D. C. Pande, and A. Bhattacharya

***Abstract*—Target scattered time domain response in the resonance region can be modelled by natural poles using the singularity expansion method (SEM). A hybrid of the conventional Extinction pulse (E-Pulse) and autoregressive (AR) method is proposed in this communication for robust discrimination of radar targets. A new target discrimination number (TDN) is suggested, which gives enhanced discrimination margin for the decision process. The limitation of the conventional E-pulse method is highlighted using time domain responses of metallic cylinders of different radii obtained through simulations. The hybrid E-pulse technique is applied to scatterers in free space as well as under the surface and demonstrated to produce comfortable discrimination margins.**

***Index Terms*—AR, EDN, E-pulse, FDTD, SEM, S-pulse, TDN.**

I. Introduction

Resonance based radar target discrimination schemes using time domain target responses have generated considerable interest in the past [1]–[3]. One of the most popular methods used in recent time for resonance based target discrimination is the E-pulse discrimination technique introduced by Rothwell *et al.*. [2]. The E-pulse discrimination number (EDN) was introduced to quantify the discrimination process for automated decision making [3]. Pulse basis functions were traditionally used for the construction of E-pulse, but recently Morales *et al.*. [4] showed that exponential basis functions give improved discrimination capacity. However, the late time response of a low SNR signal may still produce erroneous results. To overcome this limitation, the E-pulse method was applied to the early-time portion of the time domain target response (based on target scattering centers) [5].

The early time E-pulse technique requires separate waveforms for each target aspect angle and thus demands significantly more storage

Manuscript received September 04, 2013; revised May 15, 2014; accepted May 19, 2014. Date of publication May 22, 2014; date of current version July 31, 2014.

D. K. Singh and D. C. Pande are with the Electronics & Radar Development Establishment, Bangalore, India (e-mail: dhiraj_lrde@rediffmail.com; pande.dc@gmail.com).

N. Mohan is with CMR Institute of Technology, Bangalore, India (e-mail: naveena.mohan@gmail.com).

A. Bhattacharya is with theIndian Institute of Technology, Kharagpur, India (e-mail: amitabha@ece.iitkgp.ernet.in).

Color versions of one or more of the figures in this communication are available online at http://ieeexplore.ieee.org.

Digital Object Identifier 10.1109/TAP.2014.2326174